

Chapter 13

Numerical Computation Methods for Modeling the Phenomenon of Tool Extraction

B. Denkena, E.P. Stephan, M. Maischak, D. Heinisch, and M. Andres

Abstract. Tool extraction is a phenomenon, where the end mill slips out of the shrink-fit chuck in axial direction during the cutting process. This leads to severe damage of the workpiece, the tool and in some cases even the machine spindle. So far, this is an unexplained problem with no repeatability. In this article, experimental investigations such as scanning electron microscopy (SEM) and residual stress measurements on the clamping surface of shrink-fit chucks affected by tool extraction are presented. Furthermore, results from experiments on a special test-rig and a mathematical approach, which aims at the prediction of failures due to Process Machine Interaction, are described. Within the mathematical approach, a finite element model of the tool and the tool holder is linked with a cutting force simulation. The dynamic behavior of the spindle is determined by frequency response function measurements. From these measurements, a modal model is deduced and coupled with the finite element model of the tool holder. The presented mathematical model is used to compute the resulting stresses in the interface of those components due to process forces.

13.1 Introduction

Thermal shrink-fit tool holders are widely used in high speed (HSC) and high performance cutting (HPC), where high torque transmission and excellent concentricity is required [1]. The clamping mechanism of shrink-fit chucks is based on an interference fit between the chuck and the tool shank. By heating up the chuck, typically by a high-frequency inductor, the inner diameter extends and the tool can be fed into it. At cooling down, the chuck reverts to its original size and thus clamps the tool. In comparison to other tool holders the clamping forces of shrink-fit chucks are very high and concentricity typically is below $3\ \mu\text{m}$ at 3 times the tool diameter. Hence, especially for HSC milling operations, where spindle speeds exceed 10,000 rpm, shrink-fit tool holders are commonly used due to the simplicity of the tool holder's design, which contributes to its balance. There are no clamping mechanisms, which have to be counterbalanced (Fig. 13.1) [2].

Analytical dimensioning of shrink-fits can be found in DIN 7190 [3], which is adequate for calculating the main parameters such as the joint pressure and the required interference depending on the intended loads. Rondé [4] performed

extensive experimental investigations on thermal shrink fit holders and developed analytical approaches for the calculation of transferable forces and the deformation behavior of collet chucks. Furthermore, he pointed out that shrink-fit chucks are excellent for transferring the highest torque compared to the other investigated collet chucks and are therefore well-suited for HSC and HPC.

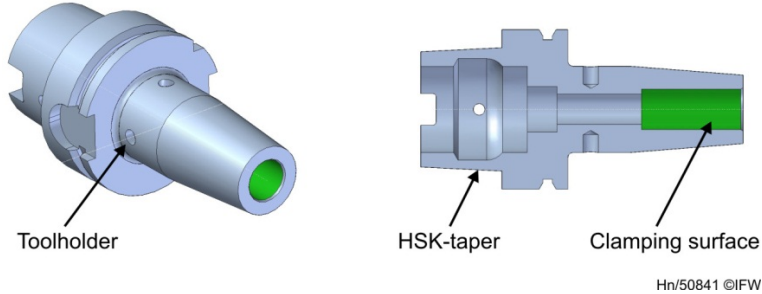


Fig. 13.1 Shrink-fit tool holder \varnothing 16 mm [Schunk]

Tool extraction is a phenomenon, where the end mill slips out of the shrink-fit chuck during the cutting process, which leads to severe damage of the workpiece, the tool and in some cases even the spindle [5, 6]. There is also the risk of injury to the worker by splintering parts. Tool extraction is a problem mainly reported from high speed or high performance cutting [7].

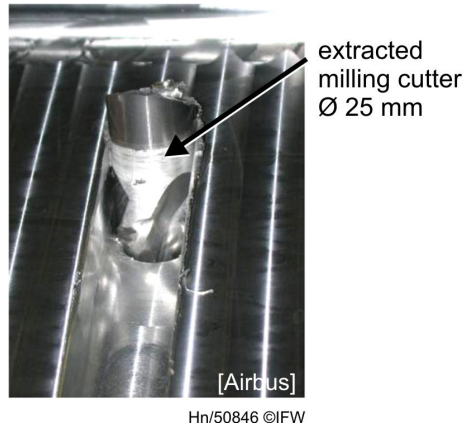


Fig. 13.2 Extracted milling cutter

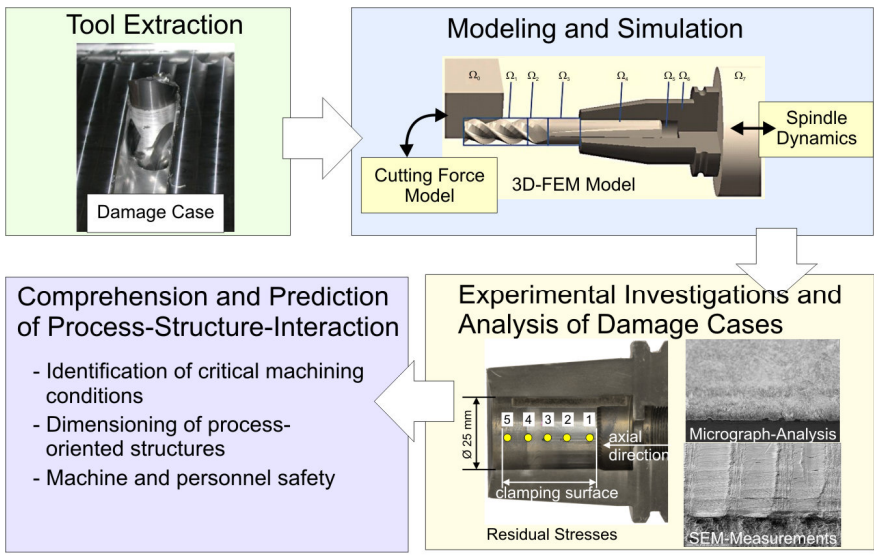
Figure 13.2 shows a milling cutter, which slipped out of the shrink-fit chuck and broke off during high speed milling of aluminum. From reported cases it is known that an extraction of several millimeters sometimes occurs after only a few minutes of operating time. In other cases, shrink-fit malfunction appeared after months of operation. Until now, no specific repeated pattern has been recognized.

The appearance of tool extraction can also not be connected to obvious chatter vibrations. Furthermore, there are no obvious faults related to the shrinking process.

Hence, the cause of this phenomenon is presently unknown but it is legitimately assumed that it is an effect from the interaction of the cutting process and the tool/tool holder/spindle dynamics. Thus, for investigating the phenomenon of tool extraction the dynamic behavior of the spindle as well as the milling process have to be considered.

Solution Approach

The objective is the comprehension and subsequently the prediction of critical machining conditions (see Fig. 13.3). Therefore, after analyzing damage cases, the phenomenon is analyzed by creating a simulation model of the tool and the shrink-fit holder. This model enables the transient calculation of the stresses in the contact zone between the tool shank and the holder’s clamping bore. The interaction with the cutting process and the spindle dynamics is performed by coupling the tool/tool holder model with a cutting force calculation on one side and a dynamic model of the spindle on the other side.



Hn/50840 ©IFW

Fig. 13.3 Solution approach

Supplementary to the simulations, experimental investigations are performed. Shrink-fit holders and tools from damage cases are analyzed. Experiments for the verification of the simulation models are carried out, and test series on a test rig are conducted to reproduce the phenomenon of tool extraction. The comprehension as to which circumstances make the interface between the tool and the tool holder fail enables the prediction of critical machining conditions.

The next section presents selected damage cases and shows results from analyses of the accordant shrink-fit holders. Furthermore, the test-rig for reproducing the tool extraction experimentally is described as well as results from those experiments. Subsequently, the simulation model of the tool and the tool holder is introduced, followed by simulation results and a short summary.

13.2 Experimental Investigations

As the phenomenon of tool extraction is not yet known in detail, the analysis of damage cases may help to understand the interaction between the tool shank and the tool holder's clamping surface. In this section, two damage cases are described, where tool extraction occurred. Furthermore, the clamping surface of several shrink-fit tool holders subjected to tool extraction has been analyzed and the results are discussed here. Finally, a test-rig for reproducing tool extraction under pre-determined conditions is shown and results are presented.

13.2.1 Damage Cases

The following damage cases occurred at high speed milling of aluminum workpieces for aerospace parts. In aerospace industry, integral components made from aluminum are widely used. To avoid joints those parts are manufactured from solid blocks. The advantage is the optimal usage of the material properties at a minimum weight. As integral components typically have a material removal rate of more than 95 %, high cutting speeds and feed rates are required for economic cutting processes. In those high speed cutting processes tool extraction is a known problem and leads to severe damage, not only to the tool and the workpiece but in some cases also to the spindle and, thus, causes a significant economic loss.

Figure 13.4 shows a workpiece of Al7075, where the tool, a $\text{Ø}25$ mm serrated end mill, slipped out of the holder by 5 mm at a revolution speed of 16,000 rpm and a feed rate of 21 m/min. The depth of cut was continuously increased by a 5° -angled tool path at 15 mm width of cut. At the corner, where the direction of feed changes by 90 degrees and an increase of the immersion angle occurs, the cutter started to move out of the shrink-fit holder in axial direction. After approximately 30 mm the cutting forces exceeded the material limits and the tool broke off. The marks on the workpiece right before the point of process interruption indicated severe vibrations of the tool. At that point, the end mill had slipped out of the shrink-fit holder by approximately 5 mm.

In contradiction to the previous case, the tool damage described in the following occurred at high performance cutting of titanium during a test series. As shown in Figure 13.5, the workpiece was machined by slot milling with an overlap of 17 mm with a $\text{Ø}25$ mm three-edged end mill. The depth of cut was 50 mm at a spindle speed of 636 rpm and a feed rate of 0.15 mm per tooth.

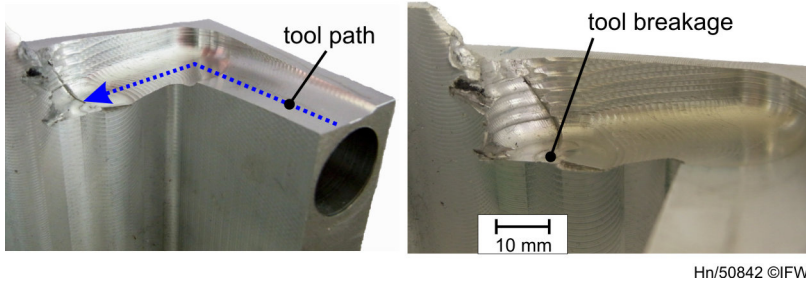


Fig. 13.4 Aluminum workpiece subjected to tool extraction

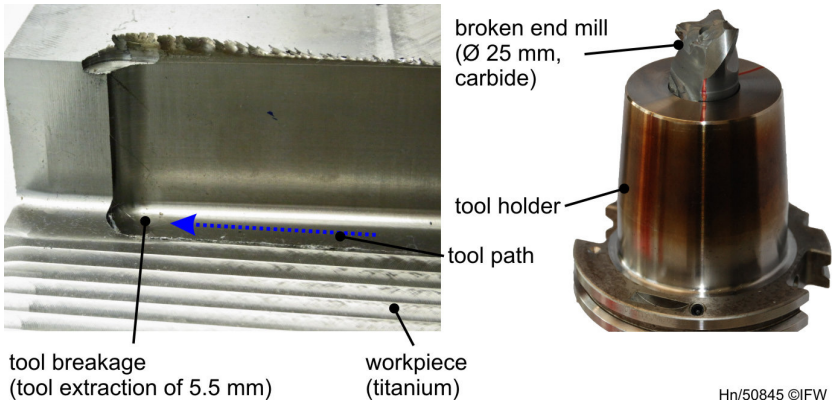


Fig. 13.5 Tool extraction at titanium workpiece and broken tool with tool holder

As titanium is a high-tensile material, machining is carried out at comparatively slow cutting speeds and the cutting forces are much higher compared to the machining of aluminum. In this case, a reinforced shrink-fit holder with a wall thickness of 17 mm was used. The interference of the tool shank and the holder is 24 μm and thus lies within the tolerance compared to other shrink-fit holders. Measurements with a tri-axial dynamometer mounted between the workpiece revealed that process forces were increasing from line to line due to increasing wear of the cutting edges.

13.2.2 Analysis of Shrink-Fit Chucks Subjected to Damage

In order to investigate the causes of tool extraction, shrink-fit holders from several damage cases were analyzed by geometry measurements, scanning electron microscopy (SEM), residual stress measurements, hardness testing as well as surface and roughness measurements. For comparison, new and normally used tool holders were also analyzed in the same manner. Measurements of the interference between tool shank and the holder’s clamping bore showed that the tool holders in the damage cases do not have significant lower interference fits than other holders.

The subsequent analyses concentrated on the clamping surface of the shrink-fit holders. Therefore, the holders were serrated into smaller parts as shown in Figure 13.6 in order to gain access to the clamping surface. With these parts surface measurements at different positions were performed using SEM. Moreover, measurements of the residual stresses in the clamping surface were performed at the five axially-ordered spots designated in Figure 13.6.

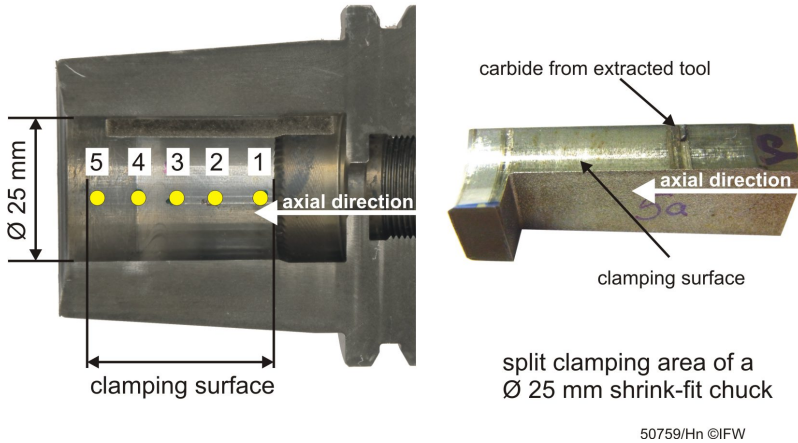


Fig. 13.6 Shrink-fit holder subjected to tool extraction

With an X-ray diffractometer of the type GE XRD 3000 P the stresses were measured in axial (x) and circumferential (y) direction. For the presented data, damaged shrink-fit chucks with different tool diameters were analyzed. The results were compared to new shrink-fit chucks and to those already subjected to several clamping cycles.

Figure 13.7 shows the mean values of the residual stresses divided into three groups. New shrink-fit chucks, those subjected to several clamping cycles for reference and holders from damage cases. Subdivided by circumferential and axial direction, mean values for each of the three groups were calculated and related to the mean stresses of the new shrink holders.

The mean stress amplitudes proved that – compared to the new and normally used – the residual stresses in holders affected by tool extraction are significantly higher than in new or normally used chucks. Especially in the circumferential direction, the residual stresses increased at a higher percentage than in axial direction. This indicates that the material properties in the clamping surface are not only affected in axial direction when tool extraction occurs but rather in circumferential direction.

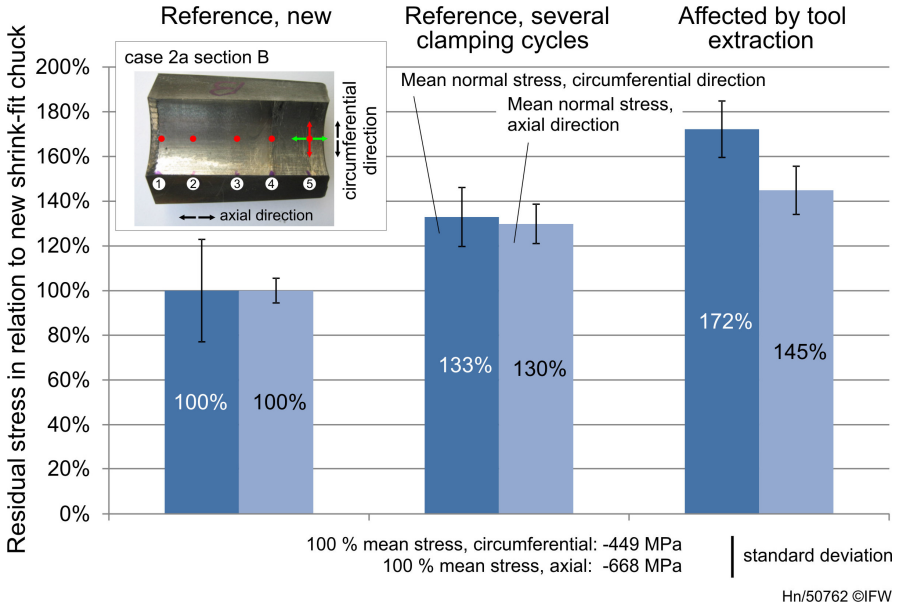


Fig. 13.7 Measurements of residual stress in clamping surfaces

Thus, with the help of SEM measurements the clamping surface is further investigated. In Figure 13.8 a) a section of the clamping surface of a shrink-fit chuck being used for several clamping cycles without tool extraction is shown. On the surface, the grinding grooves from the manufacturing process can clearly be identified in circumferential direction. Moreover, the surface is flattened due to the previously applied clamping pressure.

The bright marks on the clamping surface of the shrink-fit chuck in Figure 13.8 b), which was subjected to tool extraction, corroborate the theory of the tool shank revolving and flexing in the clamping bore and piece-wise slipping in the axial direction.

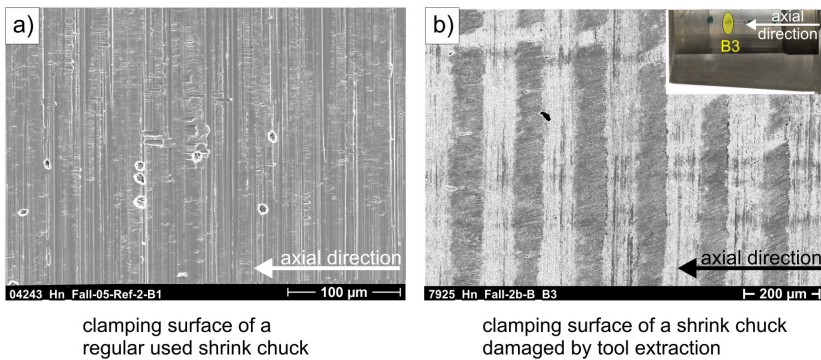


Fig. 13.8 SEM measurement of new and damaged clamping surface

Thus, neglecting thermal effects so far, it seems that not only axial slipping between tool shank and shrink-fit chuck but rather circumferential slipping is a main phenomenon when tool extraction occurs. Hence, it is assumed that, due to dynamic interaction between the tool and the workpiece, tool extraction is a combination of axial and circumferential slipping. Once static friction is lost, axial force induced by the right-handed helix angle of the milling cutter leads to a relative axial movement.

13.2.3 Experimental Investigations on Test Rig

In order to experimentally determine the dynamic conditions, which lead to tool extraction, a special test-rig has been designed and built up (Fig. 13.9). With this test-rig, different tool holders can be exposed to dynamic loads at revolution speeds of up to 20,000 rpm. The tool holder is mounted on a conventional milling spindle and a carbide cylinder is clamped in the holder as a dummy tool. The carbide cylinder itself is connected to a rotor shaft designed for transferring the loads to the tool/tool holder interface. The loads are applied via electromagnetic actuators in radial and axial direction. With a second milling spindle, connected by an axially-elastic clutch, torque loads can also be applied. The displacement of the rotor shaft is measured at the radial lamination core in radial and axial direction with five eddy current sensors. The rotational displacement between tool and tool holder is measured via rotary-pulse generators in the spindles. The test-rig is controlled via a rapid prototyping system, which allows fully-automated operation and the deterministic application of harmonic and non-harmonic load spectra.

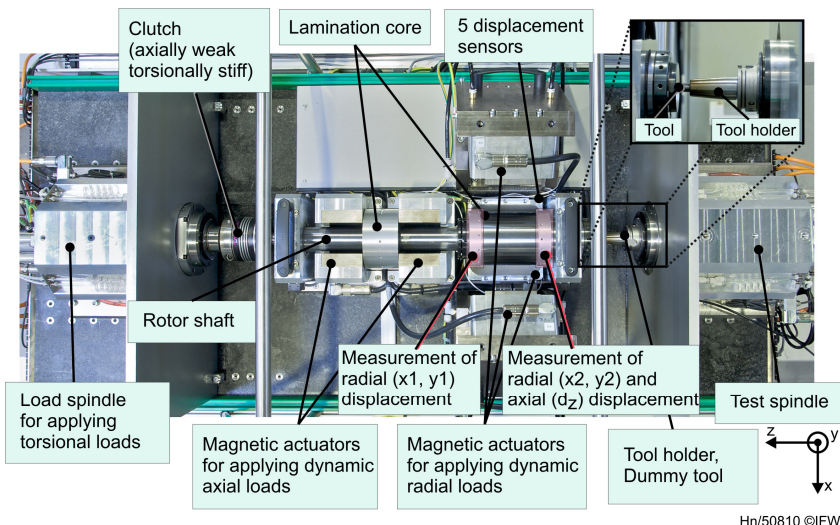


Fig. 13.9 Spindle test-rig at IFW

More than 100,000 tests were performed with diameter 12 and 16 mm tool-tool-holder combinations at usual interference fits. However, test results showed that dynamic loads applicable by the test-rig are too low to enforce shrink-fit failures in terms of relative axial or rotational displacement of tool shaft and tool-holder. This might not only be explained by the forces but also by differences in the structural dynamic behavior of the tool/tool holder/spindle assembly in the test-rig compared with that in a cutting process. Thus, widened shrink-fit chucks were used for further tests. At these chucks, the clamping bore was previously widened by honing. With this process, the cylindricity and surface quality of the clamping bore are only minimally affected as honing is also the finishing process in the production of shrink-fit chucks.

In the following, results from tests with widened shrink-fit chucks with a nominal diameter of 16 mm are presented. In these tests, tool extraction occurred under several dynamic loads. The parameters defining the dynamic load are amplitudes of radial and axial force, excitation frequency and torque. The loads in radial ($F_r(t)$) and axial ($F_a(t)$) direction are then defined as a harmonic function:

$$\begin{aligned} F_r(t) &= A_x \sin(2\pi f_x t) + F_{0,x} + A_y \sin(2\pi f_y t + \varphi_{xy}) + F_{0,y} \\ F_a(t) &= A_z \sin(2\pi f_z t + \varphi_{xz}) + F_{0,z} \end{aligned} \quad (13.1)$$

The torsional load is defined as constant (M). The interference-fit as a parameter is induced by using shrink-fit chucks with different widening. Furthermore, properties of the clamping bore have to be considered, such as cylindricity, surface roughness and the coefficient of friction between tool shank and clamping surface. During the tests, the radial, axial and angular displacement of the rotor shaft is measured. Radial displacement is measured on the left and right side of the radial laminaton core. As the measurement location on the right is closer to the tool/tool holder assembly its amplitude y_2 is used within the analysis of the test results. In Figure 13.10, the ranges of the varied parameters and the discrete parameter values are shown. As the system of rotor shaft, tool, tool holder and spindle shows frequency-dependent dynamic behavior when excited by harmonic loads, the excitation frequency is an important parameter. Within only small frequency ranges large variations in the resulting amplitude may occur. Thus, frequency is the parameter with the most variation. In order to reduce the number of experiments only few parameters were varied, as shown in Figure 13.10. Other parameters remained constant or zero, i. e. the tests were performed at a constant revolution speed of 1,000 rpm, only radial force in y-direction, constant axial force and torque.

Analyzing the amplitude y_2 (near the tool) reveals the dynamic behavior of the system under forced vibration in radial y-direction. In Figure 13.11 (top), the y_2 is plotted against the excitation frequency f_y for $A_y = 1,250$ N and $F_{0,z} = 250$ N and $M \geq 30$ Nm. The diagram clearly shows some of the resonances of the system. A modal analysis of the rotor shaft shows the first bending eigenfrequency at 130 Hz with a very high amplitude so that no tests are possible around this frequency. The second and third eigenfrequency can be found at 335 and 417 Hz, both with a similar mode shape, where bending occurs at tool and tool holder. The histogram in

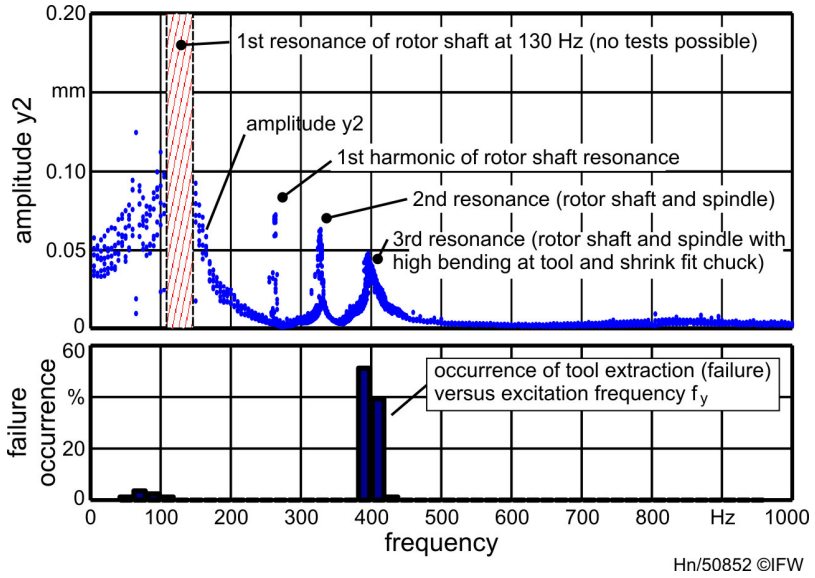


Fig. 13.11 Amplitude y_2 against frequency (top) and occurrence of failures (bottom)

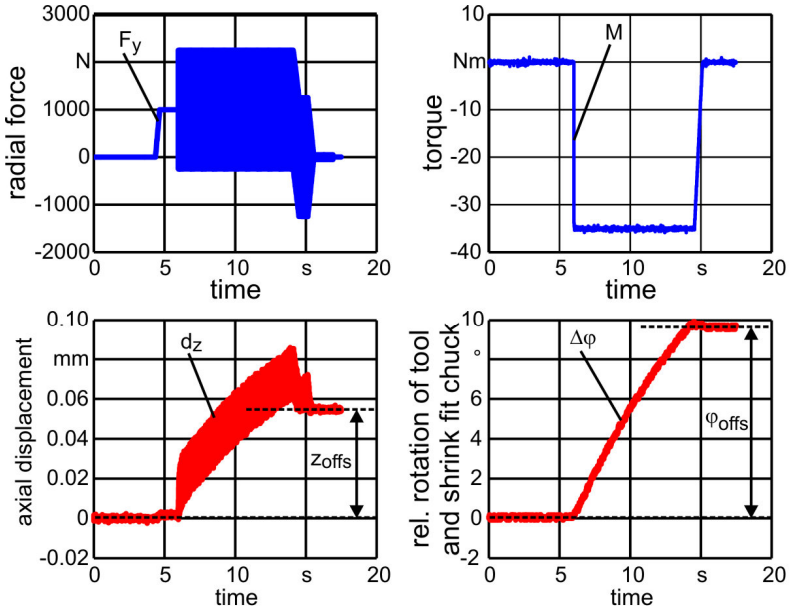


Fig. 13.12 Example of single analysis of tool extraction

In Figure 13.13, the clamping surfaces of a shrink-fit chuck subjected to experimental tests but without tool extraction (a) is compared to surfaces from shrink-fit chucks, where tool extraction occurred (b - d). In Figure 13.13a, only the grooves from honing can be seen whereas b, c and d all show significant stripes in circumferential direction, apparently caused by the revolving of the tool shank. In axial direction, no significant marks can be found. This is due to the fact that the ratio of circumferential displacement and axial displacement related to the clamping surface in all experiments with tool extraction lies between 3.5 and 20,000. The ratio tends to rise with increasing interference fit. Comparing these results with the analysis of the damage cases presented in section 13.2.2, it is assumed that in the case of tool extraction a sudden increase of torque first leads to a revolving of the tool followed by an axial movement primarily caused by axial process force. In order to understand what happens in the interface of the tool and the tool holder, finite element simulations are performed with a mathematical model of the tool and the tool holder is described in the following sections.

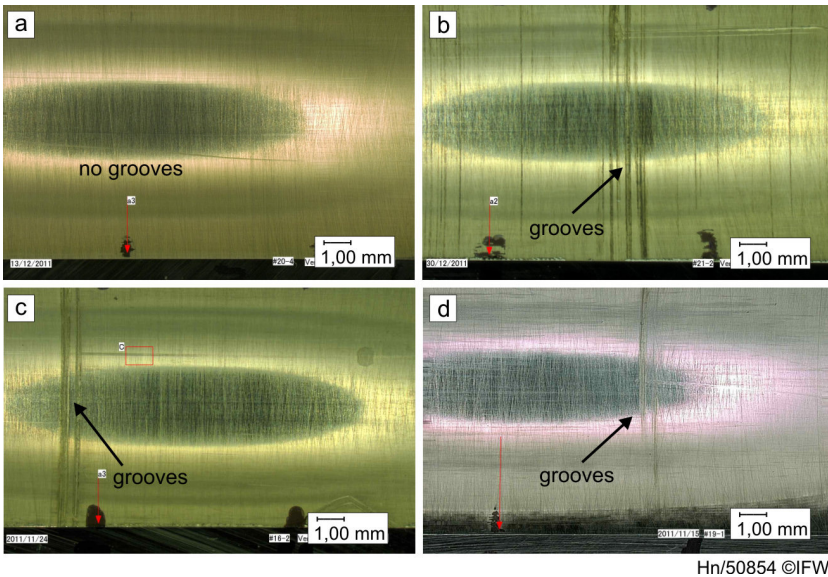


Fig. 13.13 Clamping surface of shrink-fit chuck without (a) and with tool extraction (b - d)

13.3 Mathematical Modeling

For a numerical simulation allowing the prediction of tool extraction during a cutting process a finite element model of the tool holder and the shrunk tool is essential. The governing equation describing the cutting process is the visco-elastic

wave equation. Equipped with appropriate boundary and initial conditions, the displacement field $\mathbf{u}(x,t)$ occurring in the system of tool and tool holder during the process satisfies the following boundary and initial value problem (BIVP).

$$\begin{aligned} \rho(x)\ddot{\mathbf{u}}(x,t) - \beta \operatorname{div} \sigma(\dot{\mathbf{u}}(x,t)) - \operatorname{div} \sigma(\mathbf{u}(x,t)) &= \mathbf{f}(x,t) & \text{in } \Omega \times (0,T) \\ \mathbf{u}(x,t) &= \mathbf{U}(x,t) & \text{on } \Gamma_D \times (0,T) \\ \sigma(\mathbf{u}(x,t)) \cdot \mathbf{n} &= \mathbf{T}(x,t) & \text{on } \Gamma_N \times (0,T) \\ \mathbf{u}(x,0) &= \dot{\mathbf{u}}(x,0) = \mathbf{0}. \end{aligned} \quad (13.2)$$

In the above problem, the domain Ω represents the structure of tool and tool holder and its boundary $\partial\Omega$ is decomposed into the two disjoint sets Γ_N and Γ_D . The given data is the density function $\rho(x)$, which is assumed to be independent of time. Moreover, volume forces $\mathbf{f}(x,t)$ as well as boundary tractions $\mathbf{T}(x,t)$ on the Neumann boundary part Γ_N and inhomogeneous displacements $\mathbf{U}(x,t)$ on the Dirichlet boundary part Γ_D are assumed to be given during the whole process. More precisely, the boundary tractions result from the cutting process and act at the tip of the tool and the inhomogeneous displacements result from the dynamic behavior of the spindle interacting with the tool holder. Both the cutting forces and the vibrations of the spindle were modeled separately to save a time-consuming finite element model consisting of all of the four mentioned structures (spindle, tool, tool holder and workpiece), see also the upper right image in Figure 13.3. In the following sub-sections, the finite element model of the tool and the tool holder, the model of spindle dynamics, the cutting force model and the coupling of the three models are described in detail.

13.3.1 Finite Element Model of Tool and Tool Holder

In the above BIVP, the associated material law is Hooke's law for linearly-elastic material. The tool is made of carbide and since the considered workpiece is aluminum no plastic deformations are assumed to occur in the tool or in the tool holder. A transient three-dimensional finite element model is used to approximate the BIVP for the structure of tool and tool holder. The time discretization is performed with the Discontinuous Galerkin Method (DGM), see [8], using piece-wise quadratic basis functions. Frictional contact conditions on the contact interface between tool and tool holder within the model have been neglected since the two structures are assumed to stick along the whole contact interface after the shrinking process up until critical tangential stresses are exceeded, i. e. tool extraction occurs. Hence, in the above problem, the domain Ω represents the compound of tool and tool holder owning inhomogeneous material parameters, see Figure 13.14.

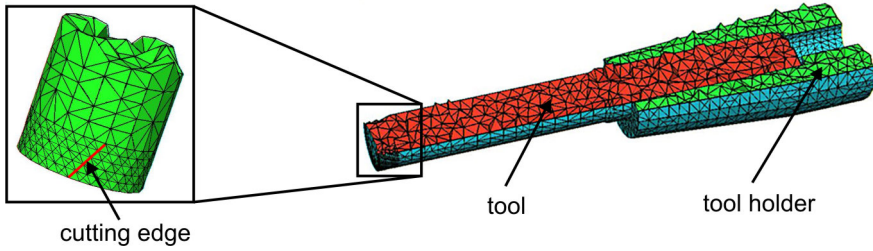


Fig. 13.14 Cross-section of the FE-model of tool and tool holder

The shrinking process is approximated by a linear heat strain law. The corresponding contact pressure is modeled by applying a negative change of temperature to the tool holder. The required temperature change is computed with the following formula

$$\Delta T = \frac{\Delta r}{\alpha_T r_i} \tag{13.3}$$

where Δr denotes the interference fit, α_T represents the coefficient of thermal expansion of the tool holder and r_i considers the inner radius of the tool holder. This approach leads to a volume force denoted by $\mathbf{f}(x,t)$ in the BIVP, which is independent of time. In the weak formulation, the volume force reads

$$\alpha_T \Delta T \psi(t) \int_{\Omega} (3\lambda(x) + 2\mu(x)) \operatorname{div}(\varphi(x)) dx \tag{13.4}$$

where $\psi(x)$ and $\varphi(x)$ denote temporal and spatial basis functions respectively and $\lambda(x)$ and $\mu(x)$ are the Lamé coefficients depending on the materials.

To simulate the process numerically a transient three-dimensional finite element method is implemented considering the close-to-process structure of tool and tool holder. Therefore, the elastic wave equation is re-written into a system of first order equations in time by introducing the velocity \mathbf{v} as an additional unknown variable such that the DGM in time can be applied

$$\begin{aligned} \dot{\mathbf{u}} - \mathbf{v} &= \mathbf{0} \\ \rho(x) \dot{\mathbf{v}}(x,t) - \beta \operatorname{div} \sigma(\mathbf{v}(x,t)) - \operatorname{div} \sigma(\mathbf{u}(x,t)) &= \mathbf{f}(x,t). \end{aligned} \tag{13.5}$$

By applying the DGM in time and standard FEM in space to the above problem, the corresponding discrete weak formulation results in a linear system of equations for the coefficients of the finite element basis functions of displacement and of velocity. To circumvent large displacements due to the rotation of the system the displacements and the velocities are described in rotational coordinates. By further applying the approach of Li and Wiberg [9] the system can be decoupled into a system concerning the velocity and three linear equations for the displacement coefficients. Finally, the stiffness matrix resulting from the divergence term in the elastic wave equation is used to approximate the material damping with damping factor β within the process. Let \otimes be the tensor product, then the two linear systems are:

$$\left[\mathbf{C}_p \otimes \mathbf{M}_p + \mathbf{C}_C \otimes \mathbf{M}_C + \mathbf{C}_A \otimes \mathbf{A} \right] \cdot \begin{pmatrix} \mathbf{v}_1 \\ \mathbf{v}_2 \\ \mathbf{v}_3 \end{pmatrix} = \begin{pmatrix} \mathbf{M}_p \mathbf{v}^- + \mathbf{F}_1 - \frac{k}{2} \mathbf{A} \mathbf{u}^- \\ \mathbf{F}_2 - \frac{k}{2} \mathbf{A} \mathbf{u}^- \\ \mathbf{F}_3 + \frac{k}{3} \mathbf{A} \mathbf{u}^- \end{pmatrix} \quad (13.6)$$

$$\begin{pmatrix} \mathbf{A} & \mathbf{0} & \mathbf{0} \\ \mathbf{0} & \mathbf{A} & \mathbf{0} \\ \mathbf{0} & \mathbf{0} & \mathbf{A} \end{pmatrix} \cdot \begin{pmatrix} \mathbf{u}_1 \\ \mathbf{u}_2 \\ \mathbf{u}_3 \end{pmatrix} = \begin{pmatrix} \mathbf{A} \mathbf{u}^- + \frac{k}{15} \mathbf{A} \mathbf{v}_3 \\ \mathbf{A} \mathbf{u}^- + \frac{k}{2} \mathbf{A} \mathbf{v}_1 + \frac{k}{2} \mathbf{A} \mathbf{v}_2 - \frac{k}{3} \mathbf{A} \mathbf{v}_3 \\ -\frac{k}{4} \mathbf{A} \mathbf{v}_1 + \frac{k}{4} \mathbf{A} \mathbf{v}_2 + \frac{k}{10} \mathbf{A} \mathbf{v}_3 \end{pmatrix} \quad (13.7)$$

Within the systems the matrix \mathbf{M}_p denotes the mass matrix, \mathbf{M}_C the mass matrix resulting from the coriolis force and $\mathbf{A} = \mathbf{K} - \omega^2 \mathbf{M}_Z$ the sum of the stiffness matrix \mathbf{K} and the mass matrix \mathbf{M}_Z resulting from the centrifugal force multiplied by the square of the revolution velocity ω . The three by three matrices \mathbf{C}_p , \mathbf{C}_C , and \mathbf{C}_A (see 13.8) are the corresponding coefficient matrices resulting from the analytical time integration of the DGM and the decoupling of the system, where φ_i are the hat basis functions and the first bubble function in time.

$$\mathbf{C}_p = \begin{bmatrix} \frac{1}{2} & \frac{1}{2} & \frac{-1}{3} \\ \frac{-1}{2} & \frac{1}{2} & \frac{1}{3} \\ \frac{1}{3} & \frac{-1}{3} & 0 \end{bmatrix}, \mathbf{C}_C = k\omega \begin{bmatrix} \frac{-2}{3} & \frac{-1}{3} & \frac{1}{3} \\ \frac{-1}{3} & \frac{-2}{3} & \frac{1}{3} \\ \frac{1}{3} & \frac{1}{3} & \frac{-4}{15} \end{bmatrix}, \mathbf{C}_A = k \begin{bmatrix} \frac{8\beta+3k}{24} & \frac{4\beta+k}{24} & \frac{-10\beta-3k}{60} \\ \frac{4\beta+5k}{24} & \frac{8\beta+3k}{24} & \frac{-10\beta-7k}{60} \\ \frac{-10\beta-7k}{60} & \frac{-10\beta-3k}{60} & \frac{30\beta+13k}{225} \end{bmatrix} \quad (13.8)$$

The time step is denoted by k and the vectors \mathbf{u}^- and \mathbf{v}^- represent the coefficient vectors of the displacement and the velocity at the end of the previous time interval respectively. Finally, the vectors \mathbf{F}_1 , \mathbf{F}_2 , and \mathbf{F}_3 correspond to the right hand side vectors resulting from the volume force and the boundary conditions. The two linear systems have to be solved in each time step.

A prediction of an extraction of the tool can be made by observing the stresses occurring at the interface of tool and tool holder during the process simulation. Using the DIN 7190 norm [3], which concerns the necessary contact pressure of shrunk tools, an extraction may be possible, if the ratio of contact pressure and tangential stresses falls below a determined bound. Of course, this may occur only locally so that experimental tests have to be made to validate the simulations.

13.3.2 Model of Spindle Dynamics

Since the spindle is not close-to-process a direct implementation of the whole structure into the transient finite element model described in Section 13.3.1 seems unnecessary. However, the dynamic behavior of the spindle may lead to deviations and vibrations of the whole system, which cannot be neglected.

For this reason, a sub-structure modeling technique using experimental modal analysis (EMA) is applied. General techniques for sub-structure modeling are described in [10–12]. Receptance coupling techniques for the tool/tool holder/spindle assembly are especially subject to numerous works related to stability prediction for cutting processes [13–20].

The model of the spindle dynamics obtained from EMA is characterized in modal degrees of freedom. In order to integrate such a model in a finite element simulation it is transformed to a model containing physical degrees of freedom referred to a virtual point **P** at the joint between the tool holder and the spindle, see Figure 13.15a.

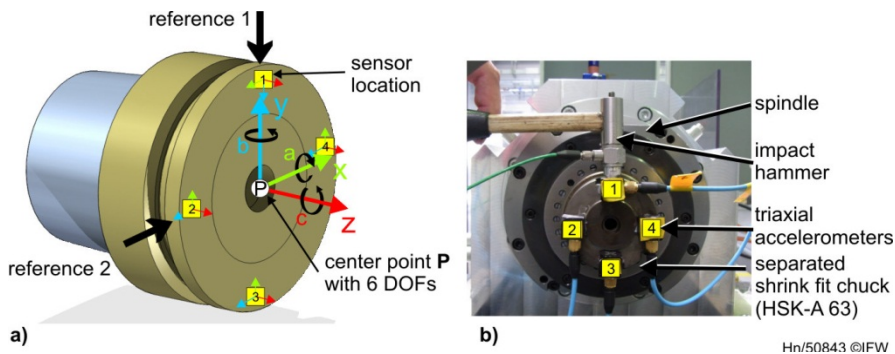


Fig. 13.15 Measurement of spindle dynamics with HSK flange from separated tool holder

To derive the model in modal degrees of freedom 24 frequency response functions (FRFs) were measured on an HSK-A-63 flange of a separated shrink-fit chuck, as depicted in Figure 13.15b. The system was excited at two reference points in radial direction by using an impact hammer with integrated force sensor. The resulting excitation of the structure was measured by four tri-axial acceleration sensors mounted on the HSK-A-63 flange. The obtained acceleration FRFs were integrated twice in order to obtain the receptances. A modal model with 34 degrees of freedom within the frequency band of 200 to 2,500 Hz was created using a poly-reference parameter estimation method.

By using the modal mass, damping and stiffness matrices \mathbf{M}_Φ , \mathbf{D}_Φ , \mathbf{K}_Φ and the incomplete mode shape matrix $\tilde{\Phi}$ obtained from the EMA, the system can be transformed into the following ordinary differential equation (ODE) with both physical and modal degrees of freedom representing the dynamic behavior of the spindle at the HSK flange:

$$\begin{aligned} \mathbf{M}_T \ddot{\mathbf{x}}(t) + \mathbf{D}_T \dot{\mathbf{x}}(t) + \mathbf{K}_T \mathbf{x}(t) &= \mathbf{F}(t) \\ \mathbf{x}(0) = \dot{\mathbf{x}}(0) &= 0 \end{aligned} \tag{13.9}$$

Within this system, \mathbf{M}_T , \mathbf{D}_T , and \mathbf{K}_T denote the transformed mass, damping and stiffness matrix respectively. $\mathbf{F}(t)$ is the force vector resulting from excitation of

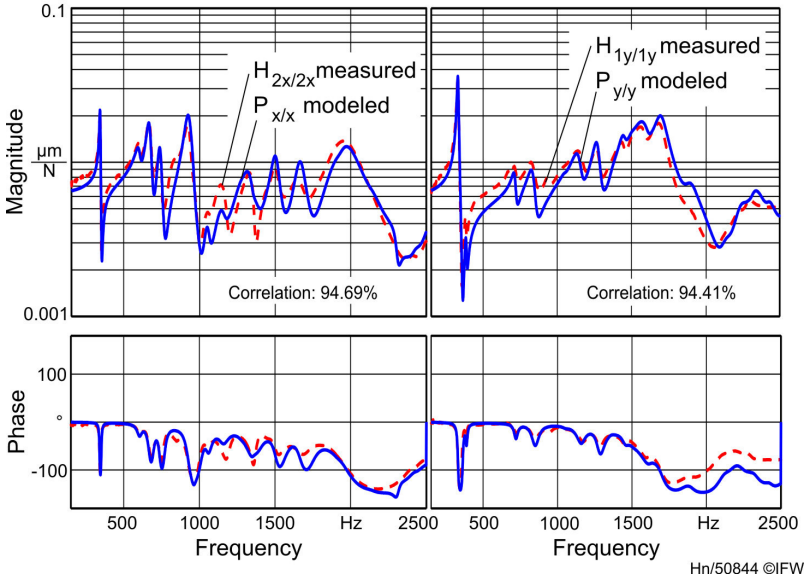


Fig. 13.16 Comparison of measured and modeled FRFs

the interface between tool holder and spindle. The first six components of $\mathbf{x}(t)$ denote the three translational and rotational degrees of freedom at the center point \mathbf{P} . Figure 13.16 compares the drive point measurements with the estimated main degrees of freedom in radial x and y-direction from the transformed modal model. As can be clearly seen, the FRFs estimated from the transformed modal model reproduce the measurements well.

13.3.3 Cutting Force Model

The boundary tractions $\mathbf{T}(x,t)$ in the BIVP resulting from the cutting process are computed by a cutting force model [21–23]. They correspond to the cutting forces of the process and are indispensable as they cause an excitation of the structure of tool and tool holder. The cutting force model is based on the assumption that the forces are proportional to the infinitesimally small cross-sectional surface A_j^i and the associated arc length b_j^i . The part of the cutting edge indenting the workpiece from the tip of the tool to the cutting depth a_p is divided into n chips, where i denotes the chip number and j the number of the cutting edge, see Figure 13.17. To compute the surface A_j^i the cutting edge trajectory is used to determine the chip thickness h_j^i . According to Altintas [24], the proportionality of the tangential, radial and axial force components \mathbf{F}_{tra} to A_j^i and b_j^i is linear and demands the

experimental determination of shear force coefficients $\mathbf{K}_{tra,c}$ as multipliers to the surface and cutting coefficients $\mathbf{K}_{tra,e}$ as multipliers to the arc length.

Once the coefficients are determined for the process the forces acting at each cutting edge j are computed to

$$\{\mathbf{F}_{tra}\}_j^i = \mathbf{K}_{tra,c} A_j^i + \mathbf{K}_{tra,e} b_j^i. \tag{13.10}$$

As the revolution velocity is assumed to be constant the tool rotation angle φ is a linear function of time t .

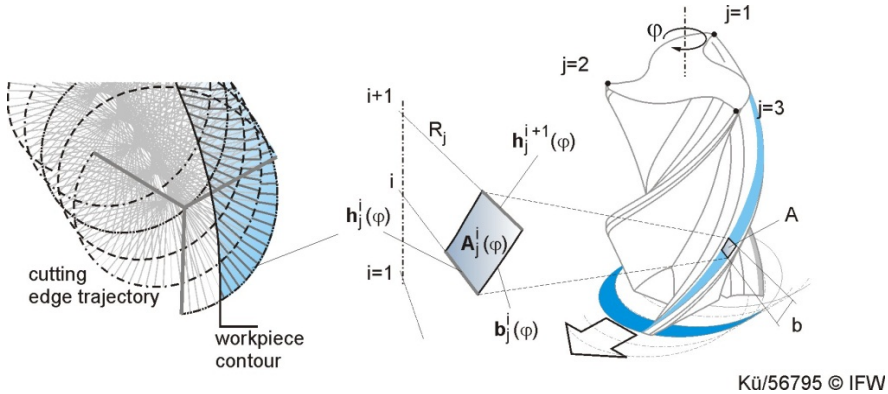


Fig. 13.17 Model for determining the cutting edge trajectories and the cutting forces [23]

If the forces are transformed into Cartesian coordinates by the transformation matrix \mathbf{T}_{tra}^{xyz} , i. e.

$$\{\mathbf{F}_{xyz}\}_j^i = \mathbf{T}_{tra}^{xyz} \{\mathbf{F}_{tra}\}_j^i \tag{13.11}$$

the corresponding process force at rotation angle φ can be computed as the sum over all chip numbers and all n_z cutting edges to

$$\mathbf{F}_{xyz}(\varphi) = \sum_{j=1}^{n_z} \sum_{i=1}^n \{\mathbf{F}_{xyz}\}_j^i. \tag{13.12}$$

However, this procedure assumes an ideal stiff tool, which is not the case in reality. For this reason, the model is extended considering self-excitations of the tool, which may be caused by the process forces. In this way, the chip thickness h_j^i is computed by considering the cutting edge trajectory at the rotation angle φ as well as a given deviation of the cutting edge at the same position and time. This will result in changes of the undeformed chip cross-section A_j^i and therefore in different process forces.

13.3.4 Coupling of the Models

To predict a possible tool extraction during a cutting process the excitation of the structure of tool and tool holder resulting from the process forces has to be taken

into account. Furthermore, the structure is affected by the vibrations of the spindle, which also result from the process forces. Hence, it is essential to couple the cutting force model on one side and the model of spindle dynamics on the other side with the transient finite element model of tool and tool holder, see Figure 13.18.

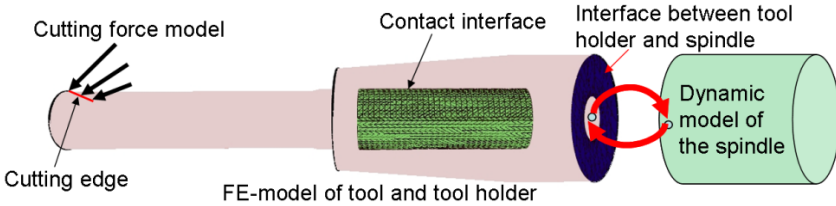
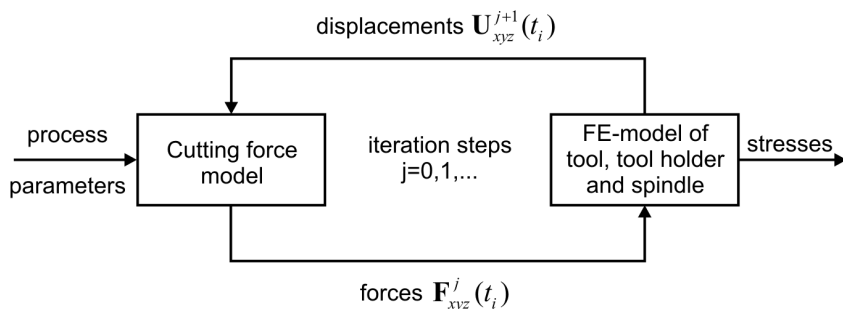


Fig. 13.18 Coupling of the models

The coupling of the process forces is accomplished via a Dirichlet-to-Neumann mapping (DEN). The cutting edges in the cutting force model are discretized as n force vectors acting on the corresponding point of the cutting edge. Therefore, the finite element mesh at the tool tip is discretized such that the element edges of the mesh follow the cutting edges in the helix angle α , see also the left image of Figure 13.18. In this way, the n force vectors can be interpolated along the edges to a line force corresponding to the boundary traction $\mathbf{T}(x,t)$ in every time step. By applying the DGM the cutting forces contribute to the three vectors \mathbf{F}_1 , \mathbf{F}_2 , and \mathbf{F}_3 on the right hand side of the system (13.6).

The implementation of the interaction of the structure of tool and tool holder with the cutting force process is explained in the following. The coupling process starts with an ideally stiff tool in the cutting force model, i. e. the deflection of the tool is $\mathbf{U}_{xyz}^0(t_0) = 0$. The starting deflection of the tool for all subsequent time steps is determined by the deflection of the previous time step. The computed cutting forces $\mathbf{F}_{xyz}^0(t_i)$ depending on the process parameters result in a deflection $\mathbf{U}_{xyz}^1(t_i)$ of the tool for every time step t_i . By using this deflection within the cutting force model in the same time step as described at the end of Section 13.3.3, the new forces $\mathbf{F}_{xyz}^1(t_i)$ are calculated with the effective tool deflection. This procedure is repeated until the residual of two consecutive forces $|\mathbf{F}_{xyz}^j(t_i) - \mathbf{F}_{xyz}^{j-1}(t_i)|$ falls below a given bound. When the iteration loop has converged, the stresses on the interface of tool and tool holder can be computed. The coupling procedure at time step t_i is visualized in Figure 13.19.



Hn/50847 ©IFW

Fig. 13.19 Coupling of the cutting force model and the FE-simulation of tool and tool holder [6]

On the other side, the vibrations of the spindle excited by the cutting forces interact with the tool holder at the corresponding interface, see Figure 13.18. When the dynamic behavior of the spindle is known in terms of the ODE (13.9), it is coupled via a DEN mapping with the FE model of tool and tool holder by the inhomogeneous Dirichlet data $\mathbf{U}(x,t)$ in the BIVP (13.2). Here, the Dirichlet boundary Γ_D is defined as the interface between tool holder and spindle. Starting with $\mathbf{U}(x,0) = \mathbf{0}$ the displacement $\mathbf{U}(x,t_i)$ is approximated by the solution $\mathbf{x}(t_i)$ of the ODE (13.9). In detail, for every x on Γ_D and every time step t_i , the corresponding displacement is the sum of the translation in the first three components of $\mathbf{x}(t_i)$ and the rotation of x around the center point \mathbf{P} with rotation angles in the fourth to sixth component of $\mathbf{x}(t_i)$

The force vector $\mathbf{F}(t)$ is necessary to solve the ODE (13.9). The deflection of the tool, which is caused by the cutting forces, results in an oscillation of the Dirichlet boundary Γ_D . Hence, the forces and moments in the first six components of the force vector $\mathbf{F}(t)$ on the right hand side of (13.9) are computed by the solution vectors \mathbf{u}_1 , \mathbf{u}_2 , and \mathbf{u}_3 of the linear system (13.7). By computing the stress tensor $\sigma(\mathbf{u})$ due to Hooke’s law, the forces and moments are computed to

$$\begin{aligned} \{\mathbf{F}(t_i)\}_{1\dots3} &:= \int_{\Gamma_D} \sigma(\mathbf{u}(x,t_i)) \cdot \mathbf{n} \, dx \\ \{\mathbf{F}(t_i)\}_{4\dots6} &:= \int_{\Gamma_D} (x - \mathbf{P}) \times (\sigma(\mathbf{u}(x,t_i)) \cdot \mathbf{n}) \, dx \end{aligned} \tag{13.12}$$

where \mathbf{n} denotes the normal outward to the Dirichlet boundary Γ_D . Since the eigenfrequencies expressed by the model of spindle dynamics are not affected by an excitation the last 28 components of $\mathbf{F}(t_i)$ are set to zero. To ensure that the correct data is exchanged within the coupling an iterative loop, as shown in Figure 13.19, is applied for every time step. This leads to a series of force vectors $\mathbf{F}^j(t_i)$. Again the inner iteration stops, if the difference of two consecutive force vectors $|\mathbf{F}^j(t_i) - \mathbf{F}^{j-1}(t_i)|$ falls below a predefined bound. The cycle for a fixed time step t_i is visualized in Figure 13.20.

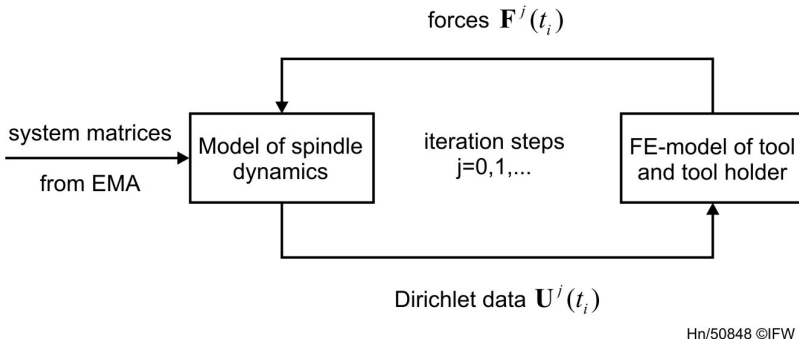


Fig. 13.20 Coupling of the spindle dynamics and the FE-model of tool and tool holder [6]

13.4 Application of Simulation Methods

To approximate a cutting process with the help of the simulation methods described in Section 13.3 the coupling of the different models has to be validated. For the coupling of the cutting force model with the finite element model of tool and tool holder the cutting forces of a cutting process are measured. These measured forces were compared with the forces resulting from the cutting force model when the coupling of the two models mentioned above is applied to the same process.

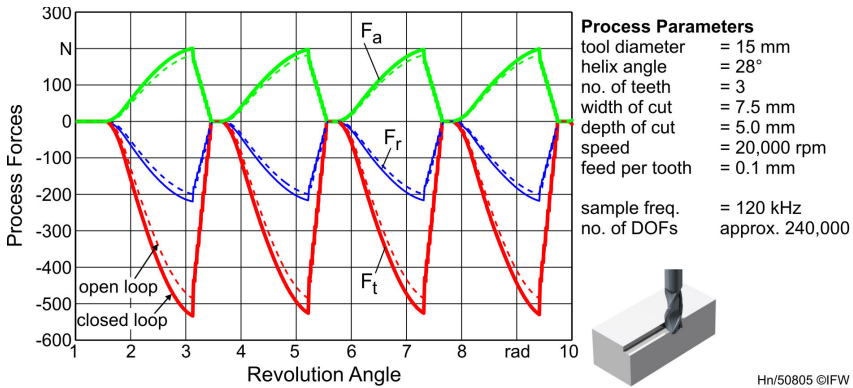


Fig. 13.21 Transient simulation of process forces considering dynamic tool deflection

The effect of the coupling, i. e. the consideration of the tool deflection within the cutting force model is visualized in Figure 13.21. The figure shows the forces in radial (\mathbf{F}_r), axial (\mathbf{F}_a) and tangential direction (\mathbf{F}_t), which act on the cutting edges of the tool during one revolution of the cutting process. The continuous lines represent the forces from the cutting force model considering tool deflections, whereas the dashed lines are computed by the cutting force model

considering an ideally stiff tool. It turns out that the consideration of the tool dynamics has significant influence on the amplitude of the cutting forces, which should not be neglected. Furthermore, effects such as regenerative chatter can only be considered, if the models are coupled.

With the help of the coupled models, simulations with various load cases are performed to investigate the stresses in the contact zone of the tool and the shrink-fit chuck. As an example, Figure 13.22 shows the change in tangential stress in axial direction related to the initial stress state of the shrunk tool during a transient process simulation for a single time step.

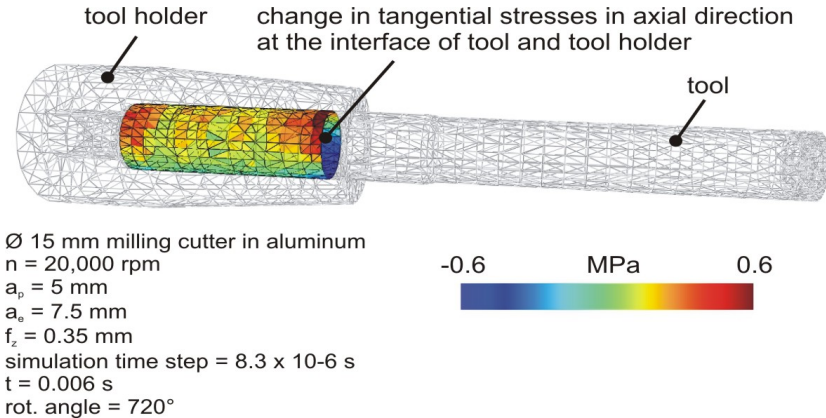


Fig. 13.22 Change in tangential stress in tool/tool holder interface due to cutting process

The prediction of relative movement of the tool and the tool holder is made possible by observing the stresses in the contact zone. If the tangential stress exceeds a certain limit defined by the normal stress and a friction coefficient tool extraction is assumed, the simulation is stopped.

Summary

The article shows experimental and mathematical approaches for the investigation of the phenomenon of tool extraction. The analysis of damage cases exhibits that tool extraction is caused by the dynamic interaction of the tool/tool holder/spindle structure with the cutting process. SEM and residual stress measurements of the clamping surface of damaged shrink-fit holders corroborate the thesis that the tool shank revolves in the clamping bore while simultaneously slipping out in axial direction. With the help of a test-rig the phenomenon of tool extraction is reproduced under various load cases and main parameters are analyzed.

Furthermore, simulations with a finite element model of the tool and the tool holder are performed concentrating on the stresses in the interface between the tool shank and the tool holder. In order to consider the dynamic behavior of

the spindle a modal model is deduced from frequency-response-function-measurements and coupled with the FE-model. The cutting process is simulated by geometrical intersection of the tool trajectory with the workpiece. The process forces are determined according to a cutting force model presented by Altintas [24]. The coupling of these models takes into account the tool deflection induced by the process forces and vice versa. Within transient simulations, the change of the stresses in the interface region resulting from the process machine interaction are computed aiming at the prediction of tool extraction.

References

- [1] Schulz, H., Rondé, U.: Werkzeuge schrumpfspannen. *Werkstatt und Betrieb* 127(11), 873–875 (1994)
- [2] Eastman, M.: Shrink-Fit Toolholding, *Cutting Tool Engineering* 49(3) (1997)
- [3] Deutsches Institut für Normung e.V., Pressverbände - Berechnungsgrundlagen und Gestaltungsregeln. Beuth Verlag, Berlin (February 2001) 17.040.10; 21.120.10/
- [4] Rondé, U.: Untersuchung von Systemen zum Spannen von Zylinderschaftwerkzeugen unter besonderer Berücksichtigung ihrer Eignung für die Hochgeschwindigkeitsbearbeitung, Dissertation, Darmstadt (1994)
- [5] Denkena, B., Stephan, E.P., Maischak, M., Heinisch, D., Andres, M.: Numerical computation methods for process-oriented structures in metal chipping. In: Denkena, B. (ed.) 1st International Conference on Process Machine Interactions, vol. 1, pp. 247–256. PZH Produktionstechn, Zentrum (2008)
- [6] Denkena, B., Stephan, E.P., Maischak, M., Heinisch, D., Andres, M., Krüger, M.: Investigations on Dynamic Tool, Structure and Process Interaction. In: Altintas, Y. (ed.) 2nd International Conference on Process Machine Interactions, Vancouver (2010)
- [7] Fladerer, F.: Haltemomente sind beim Schrumpfen ein Maß für die Produktivität. *Maschinenmarkt* 31(32), 28–29 (2007)
- [8] Johnson, C.: Numerical solution of partial differential equations by the finite element method. Dover Publ., Mineola (2009)
- [9] Li, X.D., Wiberg, N.E.: Structural dynamic analysis by a time-discontinuous Galerkin finite element method. *Internat. J. Numer. Methods Engrg.* 39(12), 2131–2152 (1996)
- [10] Duarte, M.L.M.: Experimentally derived structural models for use in further dynamic analysis, Dissertation, University of London (1996)
- [11] Ewins, D.J.: Modal testing, Theory, practice and application. Research Studies Press, Baldock (2000)
- [12] Allen, M.S., Mayes, R.L., Bergman, E.J.: Experimental modal substructuring to couple and uncouple substructures with flexible fixtures and multi-point connections. *Journal of Sound and Vibration* 329(23), 4891–4906 (2010)
- [13] Altintas, Y., Weck, M.: Chatter Stability of Metal Cutting and Grinding. *CIRP Annals - Manufacturing Technology* 53(2), 619–642 (2004)
- [14] Park, S.S., Altintas, Y., Movahhedy, M.: Receptance coupling for end mills. *International Journal of Machine Tools and Manufacture* 43(9), 889–896 (2003)
- [15] Filiz, S., Cheng, C.H., Powell, K.B., Schmitz, T.L., Ozdoganlar, O.B.: An improved tool-holder model for RCSA tool-point frequency response prediction. *Precision Engineering* 33(1), 26–36 (2009)

- [16] Schmitz, T.L.: Torsional and axial frequency response prediction by RCSA. *Precision Engineering* 34(2), 345–356 (2010)
- [17] Özsahin, O., Ertürk, A., Özgüven, H.N., Budak, E.: A closed-form approach for identification of dynamical contact parameters in spindle-holder-tool assemblies. *International Journal of Machine Tools and Manufacture* 49(1), 25–35 (2009)
- [18] Ertürk, A., Özgüven, H.N., Budak, E.: Analytical modeling of spindle-tool dynamics on machine tools using Timoshenko beam model and receptance coupling for the prediction of tool point FRF. *International Journal of Machine Tools and Manufacture* 46(15), 1901–1912 (2006)
- [19] Ahmadian, H., Nourmohammadi, M.: Tool point dynamics prediction by a three-component model utilizing distributed joint interfaces. *International Journal of Machine Tools and Manufacture* 50(11), 998–1005 (2010)
- [20] Kolar, P., Sulitka, M., Janota, M.: Simulation of dynamic properties of a spindle and tool system coupled with a machine tool frame. *The International Journal of Advanced Manufacturing Technology*, 1–10 (2010)
- [21] Clausen, M.: *Zerspankraftprognose und –simulation für Dreh- und Fräsprozesse*, Hannover (2005)
- [22] Denkena, B., Tracht, K., Schmidt, C.: A flexible force model for predicting cutting forces in end milling. *Production Engineering – Research and Development* 13(2), 15–20 (2006)
- [23] Denkena, B., Schmidt, C.: Experimental Investigation and Simulation of Machining Thin-Walled Workpieces. *Production Engineering – Research and Development* 1(4), 343–350 (2007)
- [24] Altintas, Y.: *Manufacturing automation. Metal cutting mechanics, machine tool vibrations, and CNC design*. Cambridge Univ. Press, Cambridge (2000)